Journal of Mathematical Chemistry 23 (1998) 239–260

Propagating fronts in reaction–diffusion systems

D. Vives [a], J. Armero [b], A. Martí [b], L. Ramírez-Piscina [c], J. Casademunt [b], J.M. Sancho [b] and F. Sagués [a]

[a] *Departament de Química Física, Universitat de Barcelona, Diagonal 647, 08028 Barcelona, Spain*
[b] *Departament d'Estructura i Constituents de la Matèria, Universitat de Barcelona, Diagonal 647, 08028 Barcelona, Spain*
[c] *Departament de Física Aplicada, Universitat Politècnica de Catalunya, Dr. Gregorio Marañón 50, 08028 Barcelona, Spain*

Propagating reaction–diffusion fronts constitute one of the paradigms in the realm of the nonlinear chemical phenomena. In this paper different situations are considered. Firstly, we discuss the problem of front propagation in a two-variable chemical system exhibiting multiple stationary states. Emphasis is put on the question of velocity selection. In section 3 of our contribution, the question of front propagating in spatially modulated and noisy media is addressed. Finally, we also briefly comment on the problem of reaction–diffusion fronts in non-quiescent media. In this particular scenario we simply aim at introducing the two basic propagation modes, i.e., thin versus distributed reaction fronts, that are identified in our numerical simulations.

1. Introduction

Front propagation phenomena arise in a large variety of spatially extended systems in physics, chemistry and biology [4,6,14,15]. In a general sense, the propagation of a front may be viewed as the invasion of a state by a different one. Such a situation occurs typically in systems which have been inhomogeneously prepared in steady states of different stability. Certainly the problem has a long history on its own, specially in a chemical context where they were first reported by Luther over ninety years ago [3,11]. In such a particular chemical scenario, experimental realizations of front propagation situations are abundant as can be easily verified by consulting the recently published paper by Epstein et al. [5], who briefly review some of the most genuine nonlinear chemical behaviors. On the other hand, theoretical treatments, and particularly those based on reaction–diffusion partial differential equations [7], have also configurated during these last decades a large body of literature, starting with the classical and celebrated papers by Fisher [8] and Kolmogorov [10].

In this paper, we consider different situations related to the problem of front propagation. The first addressed question refers to one-dimensional propagating fronts in a two-variable autocatalytic chemical system showing multiple stationary states. The analysis turns out to be singularly interesting for several reasons but mainly because it

enables us to really refer to an example of front propagation under conditions of strictly simultaneous multistationarity. What we mean with this statement is that within a wide and well defined range of values for the control parameters of the system, we will be dealing with situations of coexistence of three steady states of different relative stability. This opens the possibility of analyzing, for the same set of control parameters and depending on the chosen initial condition, three possible front conditions which belong to two different categories: stable/unstable and stable/metastable connections. This turns out to be singularly relevant in relation with the application of the well-known marginal stability criteria commonly invoked to predict the selected front velocity. As it will become apparent later on this is a very sensible question especially when approaching the hysteresis limit. Apart from that, the simultaneous coexistence of up to three steady states possibilitates the appearance of genuine and rather uncommon situations of propagation of multiple fronts originating from a single initial profile.

The largest body of results presented in section 2 comes from the numerical resolution of the discretized version of the set of reaction–diffusion equations on which our model for front propagation is based. However, as much as possible they are supplemented with analytical calculations. Actually it turns out that particular exact results for the front profiles and propagation velocities can be obtained both for the stable/metastable and stable/unstable connections. In addition, the band of allowed front velocities for degenerated solutions, typical of the invasion of an unstable state by a stable one under not sufficiently localized initial conditions (“non-compact support”), can be also analytically calculated.

In section 3 we consider a generic reaction–diffusion front which propagates either two-dimensionally under a spatial modulation of the local front velocity or one-dimensionally but subjected to spatio-temporal fluctuations. In the first case we present analytical and numerical results which give the final steady state velocity and front shape. Both arise from a non-trivial interplay between the local curvature affects and the global competition process between different maxima of the local velocities. When dealing with a noisy environment, we introduce external fluctuations (colored Gaussian noise) which preserve the connected steady states but play a major role in the front interface. The final conclusion is that the velocities are systematically enhanced by a factor directly related to the noise intensity.

In section 4, the examined scenario corresponds to a reaction–diffusion front propagating in a non-quiescent but turbulently stirred medium. In this regard, stirring is numerically simulated by using a sort of “synthetic turbulence” generator. We simply comment on the pair of distinctive propagation regimes which are identified in our simulations: the thin front regime, characteristic of a distorted although still sharp interface, and the distributed reaction front regime. In both cases the front speed is enhanced with respect to propagation in a non-advected medium.

2. Fronts in a multistationary chemical system

2.1. The chemical model

Over thirty years ago, Sel'kov [21] proposed a simple kinetic model of an open monosubstrate enzyme reaction which was intended to reproduce some features of the self-oscillatory behavior observed in glycolisis. Actually, on what follows we will refer to a reduced and partially irreversible version of that chemical scheme [24]

$$A \underset{k_{-1}}{\overset{k_1}{\rightleftharpoons}} X, \qquad X + 2Y \overset{k_2}{\rightarrow} 3Y, \qquad Y \overset{k_3}{\rightarrow} B. \tag{1}$$

Convenient redefinitions of the time and concentration variables enables us to write the dimensionless forms of the rate equations appropriate to (1) as

$$\begin{aligned} &x \equiv \left(\frac{k_2}{k_3}\right)^{1/2} X, \qquad y \equiv \left(\frac{k_2}{k_3}\right)^{1/2} Y, \qquad t \equiv k_3\tau, \\ &\alpha \equiv \frac{k_1}{k_3}\left(\frac{k_2}{k_3}\right)^{1/2} A, \qquad \gamma \equiv \frac{k_{-1}}{k_3}, \\ &\begin{cases} \mathrm{d}x/\mathrm{d}t = \alpha - \gamma x - xy^2, \\ \mathrm{d}y/\mathrm{d}t = xy^2 - y, \end{cases} \end{aligned} \tag{2}$$

in terms of the two basic control parameters α and γ.

2.2. Homogeneous steady states: existence and stability

It is a simple analytical matter to find the steady states corresponding to the just given pair of kinetic equations. Apart from the always existing solution corresponding to the absence of the autocatalytic species, $x = \alpha/\gamma$, $y = 0$, the most important feature is that additional stationary solutions appear and coexist beyond an hysteresis limit given by $\alpha^2 = 4\gamma$. Moreover, when existing, the three steady states of the system lay on a straight line defined by

$$y_{\mathrm{SS}} = \alpha - \gamma x_{\mathrm{SS}}. \tag{3}$$

Explicit expressions for these two non-trivial steady states read

$$\begin{aligned} x_{\mathrm{SS2}} &= \frac{\alpha + \sqrt{\alpha^2 - 4\gamma}}{2\gamma}, \qquad y_{\mathrm{SS2}} = \frac{\alpha - \sqrt{\alpha^2 - 4\gamma}}{2}, \\ x_{\mathrm{SS3}} &= \frac{\alpha - \sqrt{\alpha^2 - 4\gamma}}{2\gamma}, \qquad y_{\mathrm{SS3}} = \frac{\alpha + \sqrt{\alpha^2 - 4\gamma}}{2}, \end{aligned} \tag{4}$$

and are represented in terms of the pair of control parameters in figure 1.

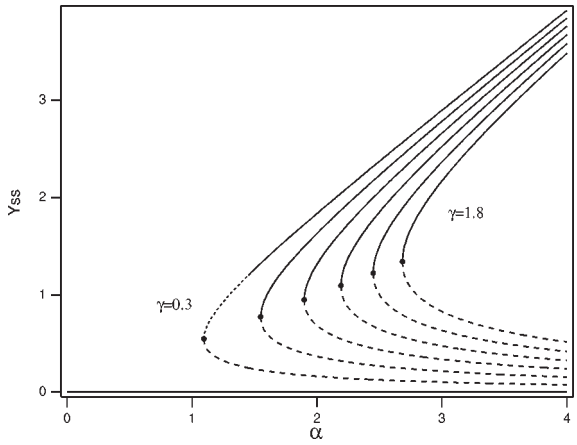

Figure 1. Plots of the steady state solutions for the concentration of the autocatalytic species Y in the irreversible version of the Sel'kov model. Solid lines refer to linearly stable solutions, whereas broken and dotted lines represent unstable determinations. Note, in particular, that the intermediate solution y_{SS2} corresponding to steady state SS2 is always unstable, whereas y_{SS3} for SS3 behaves mostly as stable except when approaching the hysteresis limit for small values of γ, where it becomes unstable (see text).

A straightforward linear stability analysis can be applied to the previously identified steady states. Classifying them simply in terms of the corresponding concentration of the autocatalytic species, the outcome of such an analysis is summarized as follows. The null y-steady state, denoted SS1 hereafter, is always a stable node. The steady state of intermediate y-values, denoted SS2, behaves as a saddle point. Finally, the steady state of large values of y, denoted SS3, shows, depending on the values of α and γ, a very rich dynamical behavior, including stable and unstable, either node or focus, characteristics. The whole phase diagram is displayed in figure 2. A typical plot of the eigenvalues corresponding to such an analysis for SS2 and SS3 is shown in figure 3. Just in passing, and totally according to what was anticipated in the introduction, we should emphasize at this point that all the front propagation conditions that are going to be discussed later on correspond to situations for which SS3 is a stable fixed point and for most of them behaving as a node.

2.3. One-dimensional fronts: model and algorithmic details

Spatial degrees of freedom are simply incorporated into our model by writing down the pair of coupled reaction–diffusion equations appropriate to the previously introduced kinetic scheme. Following a convenient spatial adimensionalization, and in terms of the ratio of diffusion coefficients δ, $\delta = D_x/D_y$, these two equations read

$$\begin{cases} \partial x/\partial t = \alpha - \gamma x - xy^2 + \partial^2 x/\partial \zeta^2, \\ \partial y/\partial t = xy^2 - y + (1/\delta)\partial^2 y/\partial \zeta^2. \end{cases} \tag{5}$$

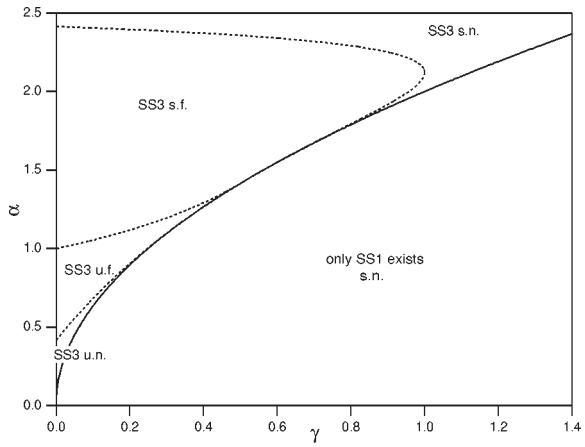

Figure 2. Phase diagram displaying the three steady states of the system in terms of their stability properties. The solid line represents the hysteresis limit $\alpha_{\rm hys}(\gamma) = 2\gamma^{1/2}$. Broken lines separate regions with different stability properties for the SS3 steady state: s(u).n., stands for stable (unstable) node and s(u).f., denotes stable (unstable) focus.

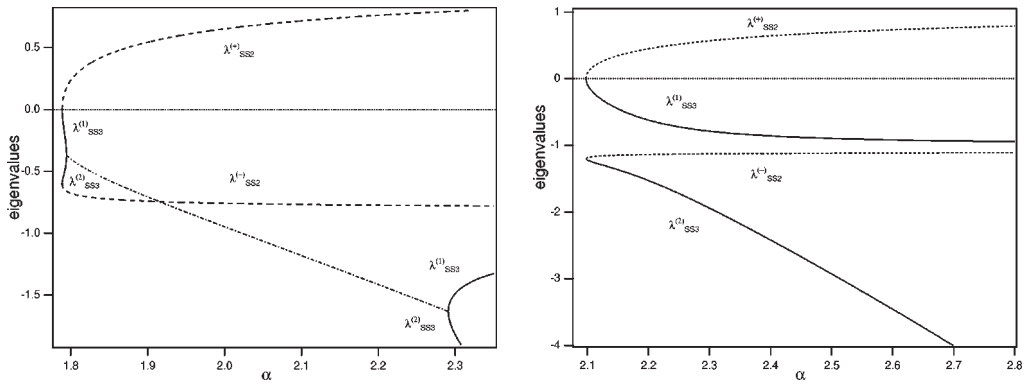

(a) (b)

Figure 3. Eigenvalues corresponding to the linear stability analysis for steady states SS2 and SS3 plotted versus α for two values of γ. (a) For $\gamma = 1.1$, SS3 is a stable node; (b) for $\gamma = 0.8$, SS3 is born from the hysteresis limit as a stable node which turns into a stable focus (only the negative real part is depicted) and, finally, converts again into a stable node.

The discretization procedure applied to (5), is based on a first order Eulerian scheme for the time derivative and centered forms for the Laplacian operator. A typical propagating front evolving from a step-like initial condition is presented in figure 4. After a normally quite short transient regime, an invariant profile connecting the pair of steady states is established and advances with a constant velocity. Initial conditions different from those represented in that figure, i.e., non-localized distributions rather than step-like profiles, will also deserve much attention on what follows. They are

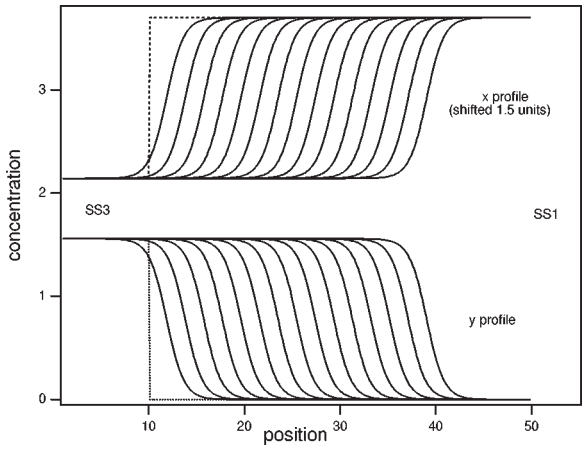

Figure 4. Typical propagating front connecting the two steady states SS1 and SS3, initiated with a step-like profile (localized distribution or compact support). The two concentration variables are shown in the plot, the x-values shifted 1.5 units to avoid overlapping with the y-profile. The chosen values of α, γ and δ are: $\alpha = 2.2$; $\gamma = 1.0$; $\delta = 1.0$. Fronts are typically separated by an amount of 10000 Δt.

prescribed according to simple exponential profiles

$$x(\zeta,0)=\begin{cases} x_{\mathrm{SS}i}, & -\infty<\zeta\leqslant 0,\\ x_{\mathrm{SS}j}+(x_{\mathrm{SS}i}-x_{\mathrm{SS}j})\mathrm{e}^{(-k\zeta)}, & 0<\zeta<\infty,\end{cases}$$
$$y(\zeta,0)=\begin{cases} y_{\mathrm{SS}i}, & -\infty<\zeta\leqslant 0,\\ y_{\mathrm{SS}j}+(y_{\mathrm{SS}i}-y_{\mathrm{SS}j})\mathrm{e}^{(-k\zeta)}, & 0<\zeta<\infty.\end{cases} \tag{6}$$

Obviously, the propagation velocity has a trivial sign degeneracy depending on the respective localization of the pair of opposed steady states. Positive values are arbitrarily chosen on most of what follows to represent the invasion from left to right, along the distributed system, of an unstable or metastable state by a more stable one.

2.4. Numerical results

As occurs in most of the situations dealing with front propagation, significatively different results are obtained for the propagation velocities and front profiles when respectively starting from localized or contrarily with distributed initial profiles connecting the pair of confronted steady states. Consequently, we are going to describe both situations separately on what follows.

2.4.1. Localized initial conditions

Restricting ourselves, as anticipated, to situations with multiple stability, two different stable/unstable connections linking SS1 or SS3 to the invaded unstable state SS2 can be considered. Results for the propagation velocities in both cases are respectively shown in figure 5 (a) and (b), in terms of the pair of control parameters α and γ. In

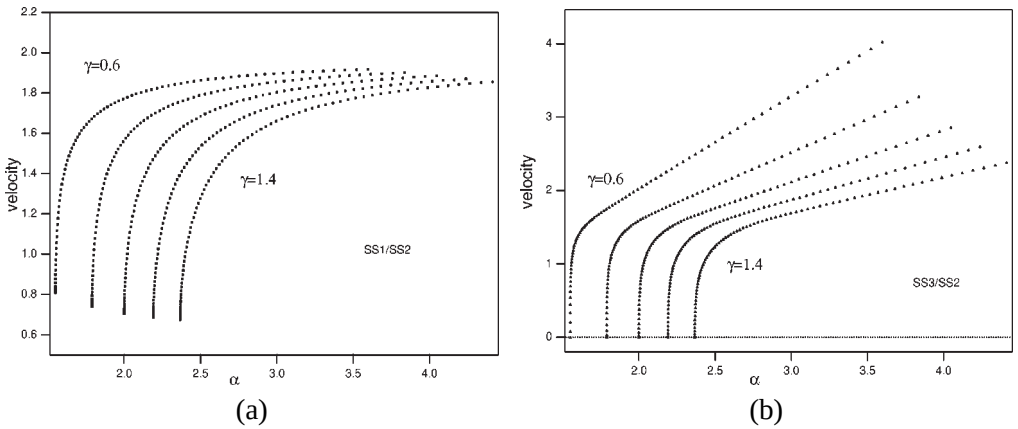

Figure 5. Front propagation velocities plotted versus α for different values of γ corresponding to the invasion of the unstable state SS2 by a stable one. (a) Connection SS1/SS2; (b) connection SS3/SS2. All the results correspond to equal diffusivities ($\delta = 1.0$).

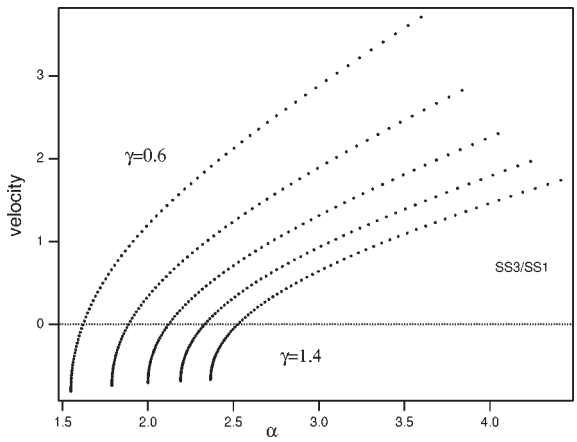

Figure 6. Front propagation velocities plotted versus α for different values of γ corresponding to the connection SS3/SS1. All the results correspond to equal diffusivities ($\delta = 1.0$).

that figure and on all what follows, unless otherwise stated, we assume a condition of equal diffusivities for the pair of intermediates, i.e., $\delta = 1$.

Now we turn to the connection between the two stable states SS1 and SS3. The corresponding results, presented analogously as in figure 5, are now summarized in figure 6 for the distribution SS3/SS1 (the notation is not arbitrary in this case since both steady states are now stable: we choose to locate SS3 at the left, whereas SS1 extends to the right). The most important feature to be noticed here is the clear signature we found of exchange of stability between these two steady states which is nicely exhibited in terms of a velocity reversal. In other words, for each value of γ, there exists a singular value $\alpha^*(\gamma)$ such that $v(\alpha^*) = 0$. According to the previously introduced notation, we clearly conclude that for most of the considered situations the

null y-steady state SS1 behaves as the mestastable state, whereas SS3 acts as the stable one.

2.4.2. Non-localized initial conditions

We turn now to the situation with non-localized initial conditions. Here we are forced to distinguish between a connection linking a stable and a metastable state from the complementary situation opposing a stable and a unstable steady state. In the first case, regardless of the initial preparation of the distributed system, the propagating front rapidly attains the steady profile and advancing velocity corresponding to the step-like initial condition examined in the previous subsection.

The situation is rather different when a stable state extends in front of a unstable one. Actually, in this case, sometimes referred in the literature as non-compact support, we encounter for the first time the well-known situation typical of many front propagation problems, where different solutions may exist within a continuous band of allowed velocities. Such a band of permitted velocities actually correspond to stable profiles with different spatial decays. This is precisely the contents of figure 7. Assuming that the propagation velocity is going to be univocally determined by the spatial decay at the leading edge of the front, which according to the initial distribution (6) is exponentially parametrized in terms of a wavenumber k, the front velocity is found to monotonously decrease as the profile gets steeper. Moreover, there is a minimum value $v^\dagger$ adopted at a particular k-value, $k^\dagger(\alpha,\gamma)$. This minimum value, on the other hand, is the one selected starting with initial conditions decaying faster than $\exp(-k^\dagger x)$ (compact support), and in particular, coincides, as it should be, with the corresponding value for the step-like initial profiles considered earlier.

2.5. Analytical results

Theoretical calculations in the context of front propagation often supposes a quite involved task. However, some strategies can be followed. First of all, exact solutions for the front profiles and velocities can be always calculated for the particular case $\gamma = 1$. Although this outcome may appear at first thought as a rather limited success, it turns out that such an exact calculation suffices to illustrate, as explained below, the crucial question of the velocity selection. Secondly, the band of allowed velocities, for general values of α and γ, in the case of distributed initial conditions extending over a unstable state admits a rather simple evaluation in terms of a linearization procedure.

2.5.1. Exact solution for $\gamma = 1$

An exact calculation of the propagating front solution can be obtained in this case by employing an ansatz of reduction of order [16,20,25]. This method basically assumes that the profile obeys a first-order differential equation with some additional constraints prescribed in order to satisfy the boundary conditions. The general solution

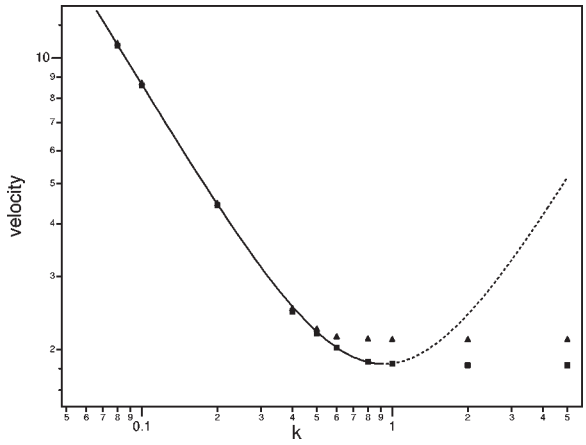

Figure 7. Front velocities corresponding to the pair of stable/unstable connections for distributed initial conditions and equal diffusivities ($\delta = 1.0$). Initial distributions are prescribed in terms of an exponential fall-off parametrized by a wavenumber k (see text). Symbols correspond to numerical results, whereas the lines either continuous (stable solutions) or broken (unstable solutions) correspond to the analytical prediction arising from a linearization procedure (see equation (16)). Squares (resp., triangles) stand for the connection SS1/SS2 (resp., SS3/SS2). The chosen values of α and γ are $\alpha = 3.0$ and $\gamma = 1.0$.

for the velocity is then given by

$$v = \frac{1}{h}\left[-\alpha + \frac{3}{2}(y_{-\infty} + y_{\infty})\right], \quad h^2 = 1/2. \tag{7}$$

When specializing it to the pair of stable/unstable connections and to the stable/metastable one, one has respective explicit expressions for the velocities which read

$$\text{SS1/SS2:} \quad v_{nl} = \frac{1}{2\sqrt{2}}\left(\alpha + 3\sqrt{\alpha^2 - 4}\right), \tag{8}$$

$$\text{SS3/SS2:} \quad v_{nl} = \alpha/\sqrt{2}, \tag{9}$$

$$\text{SS3/SS1:} \quad v_{nl} = -\frac{1}{2\sqrt{2}}\left(\alpha - 3\sqrt{\alpha^2 - 4}\right). \tag{10}$$

2.5.2. Velocity degeneracy for propagation over unstable states

Rather than to obtain simultaneous explicit expressions for the advancing velocities and front profiles, a commonly impracticable task for distributed initial conditions, we limit ourselves here to simply evaluate front velocities for stable/unstable connections. The idea is to use a linearization procedure applied to the leading edge of the front [19]. The final outcome is a sort of dispersion relation, which gives the front velocity in terms of the spatial exponential fall-off of the front profile extending into the unstable state. Since the calculation is rather straightforward, we simply give the

final result which is readily expressed in terms of the positive eigenvalue of the SS2 steady state

$$v_l(k) = \frac{k^2 + \lambda^{(+)}_{\mathrm{SS2}}}{k},$$
$$\lambda^{(+)}_{\mathrm{SS2}} = \frac{1}{2}\left\{1 - \frac{\left(\alpha - \sqrt{\alpha^2 - 4\gamma}\right)^2}{4} - \gamma + \left[\frac{\left(2 - \alpha^2 + \alpha\sqrt{\alpha^2 - 4\gamma}\right)^2}{4} - \left(\alpha - \sqrt{\alpha^2 - 4\gamma}\right)^2 + 4\gamma\right]^{1/2}\right\}. \tag{11}$$

In figure 7, this result is compared with the front propagation velocities numerically calculated for the the two stable/unstable connections. The minimum value of the velocity, $v^\dagger$, and corresponding asymptotic spatial decay, $k^\dagger$, are also easily evaluated from equation (11). Explicit expressions read

$$k^\dagger = \sqrt{\lambda^{(+)}_{\mathrm{SS2}}}, \qquad v^\dagger = 2\sqrt{\lambda^{(+)}_{\mathrm{SS2}}}. \tag{12}$$

Two main comments are now in order. First of all, note that the right branch of predicted velocities are never realized in our numerical simulations. They would correspond to unstable solutions according to the arguments of Van Saarloos [19]. It is then easy to understand the general velocity selection principle: for sufficiently localized initial conditions (compact support), the dynamically selected velocity corresponds to the speed of the stable front propagating with the steepest decay to the unstable state. As far as the velocity is dynamically selected through this simple linearization principle, such an advancing front adapts its asymptotic spatial fall-off to the value of $k^\dagger$ and its velocity is given by $v^\dagger$. This is what is known in the literature as the linear marginal stability criterion for velocity selection.

However, there is an important remark to be made in relation with this last statement. It is just a matter of comparing the results for the two possible stable/unstable connections. Note in this sense that for the particular values of α and γ considered in figure 7, most of the stable left branch of allowed velocities do really represent front connections of the unstable state SS2 with the stable one, this last one irrespectively of being the SS1 or the SS3 state: the velocities totally coincide in both cases. However, note also that some clear discrepancies appear close to the minimum velocity. Evenmore, one should notice that such a value itself does not reproduce the connection SS3/SS2.

This apparent failure is not at all fortuitous and admits a clear interpretation in terms of the so-called nonlinear marginal stability criterion [20]. According to his analysis, there are indeed situations in which the linear marginal stability criterion mentioned above fails. Then, the velocity is selected according to the nonlinear version of such marginal stability criteria. As it is clearly exhibited in figure 7, for the values of the system parameters there chosen, the connection SS1/SS2 follows the linear

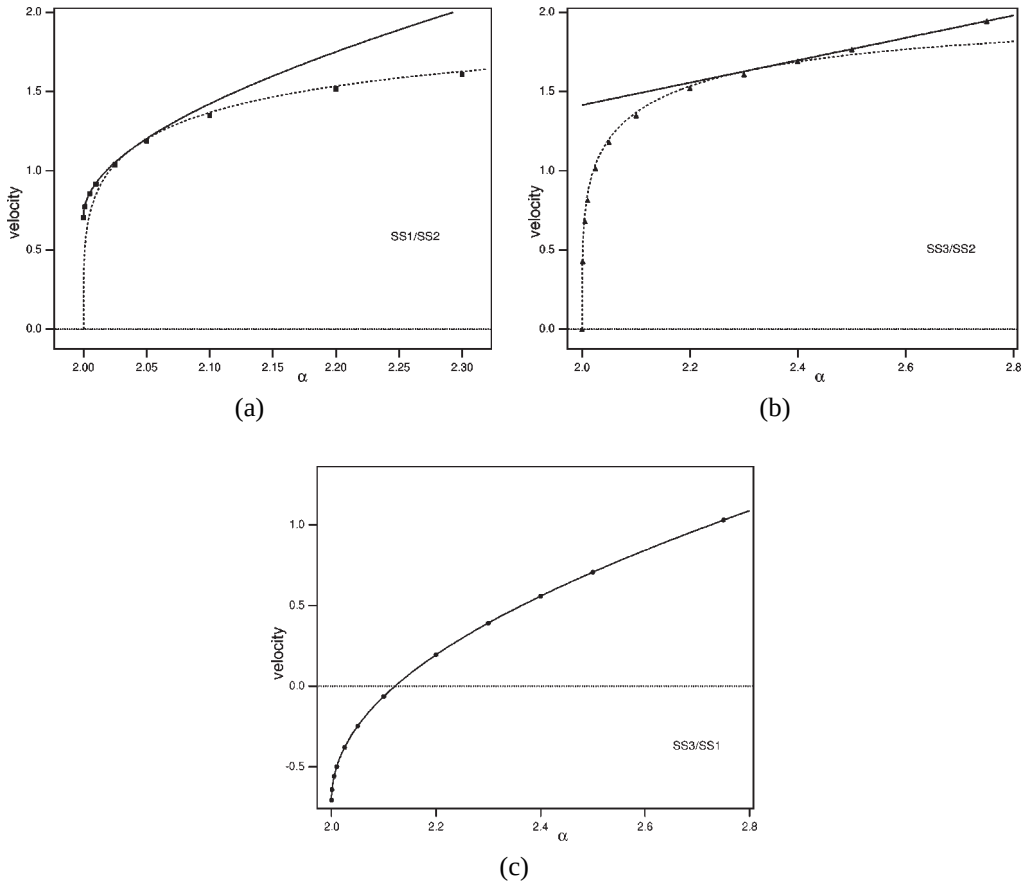

Figure 8. Front velocities corresponding to the three possible connections: SS1/SS2 (a), SS3/SS2 (b) and SS3/SS1 (c), for $\gamma = 1.0$, plotted against α ($\delta = 1.0$). Symbols stand for numerical simulations. Continuous lines represent the full nonlinear exact solutions (see equations (13)–(15)), whereas broken lines correspond to the analytical solutions obtained from a linearization procedure (see equation (17)).

marginal stability criterion for selecting the front velocity, whereas, contrarily, the nonlinear version applies to the front SS3/SS2.

The remaining question is then obvious and refers to whether or not the assignment just made for the pair of front connections to their respective velocity selection principle is a sort of general conclusion or rather depends on the particular chosen values of the system parameters α and γ. At this point, the knowledge of the exact,nonlinear, solution for $\gamma = 1$ turns out to be crucial. In figure 8, we compare the exact velocities, (7), and those obtained with our linearization procedure with the numerical calculations of the front velocities for this particular value of γ and different values of α. The comparison extends to every possible front connection, i.e., to the pair of stable/unstable and to the stable/metastable front situation. Specially remarkable to the light of the discussion in the last paragraph are the results of figure 8 (a) and (b). According to the results in this figure, it is clearly verified that there is an exchange

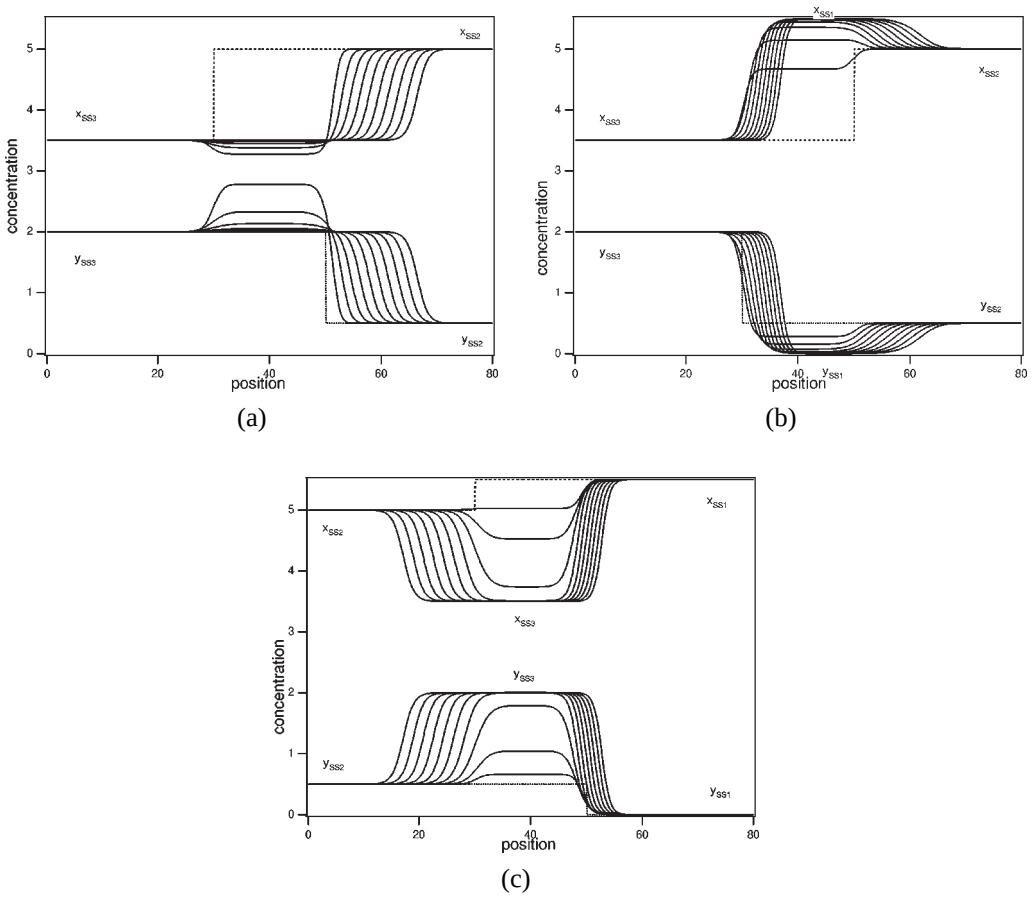

Figure 9. Front propagation conditions originated from spatially shifted initial step-like profiles. Case (a) corresponds to a single front, whereas (b) and (c) show double front propagation conditions. In (b), the two fronts propagate consecutively, whereas in (c) they separate apart. The x-values are arbitrarily shifted in the ordinates to avoid overlapping with the concentrations of the autocatalytic species. In the three cases $\alpha = 2.5$, $\gamma = 1.0$ and $\delta = 1.0$

between the role of both marginal stability criteria in selecting the front velocity when varying α. Being more specific, we conclude that the connection SS1/SS2 follows for most of the α values the linear solution, except close enough to the hysteresis limit where the nonlinear criterion applies. The situation is just the opposite one for the front SS3/SS2, since there the nonlinear criterion prevails, except again close enough to the hysteresis conditions, where, this time, the linear solution is the relevant one.

As a final comment, let us remark that this conclusion completely agrees with a statement formulated by Van Saarloos [20]), who proved that the linear marginal stability criterion is generally valid near a supercritical bifurcation (or continuous transition), while front propagation close to a subcritical bifurcation (or first order transition) is going to be generally governed by nonlinear marginal stability considerations. Accord-

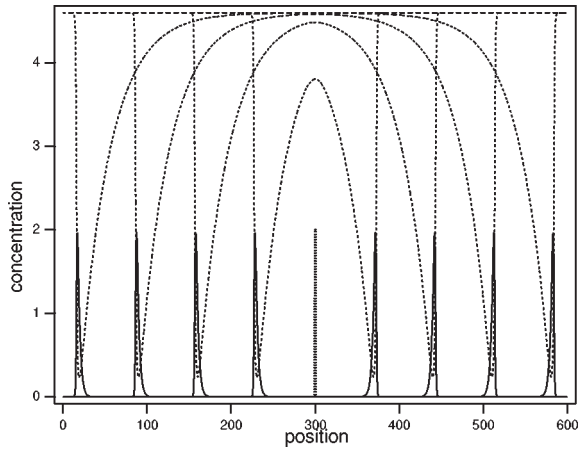

Figure 10. Pulse propagating over SS1 steady state under excitability conditions. The y-profiles are represented by continuous lines, whereas those of the x-variables are here depicted by dotted lines. The initial condition only refers to the autocatalytic species and, at is shown, is placed at the center of the distributed system. The conditions are $\alpha = 0.23,\ \gamma = 0.05$ and $\delta = 1.0$.

ing to figure 1, it is obvious that close to the hysteresis limit one could say that the SS1 and SS2 steady states are somewhat connected through a discontinuous transition, whereas, by definition, SS3 and SS2 continuously merge at that limit. Just the opposite behavior would apply to the limit of large values of α.

2.6. Other phenomenology

As mentioned in the introduction, in the course of our work we found particular conditions, either referring to the initial conditions or to the prescribed values of α and γ, which originated peculiar spatio-temporally evolving patterns. We classify them in two different categories: (i) double fronts, and (ii) pulse propagation.

2.6.1. Double fronts

The fact that we are dealing with a two-variable system, enables us to consider a specific choice of initial conditions corresponding to step-like but, this time, shifted spatial profiles for the pair of chemical species. Some specific examples are depicted in figure 9. Under these circumstances we can detect situations of double fronts either propagating in the same direction or separating each other as time goes on.

2.6.2. Pulse propagation

Sel'kov's model shows excitability properties around SS1 for very small values of α and γ. The same behavior is observed in the irreversible version considered here. Following then a localized initial perturbation on this steady state, a pulse-like solution propagates with a very sharp profile as illustrated in figure 10.

3. Front propagation in spatially modulated and noisy media

Just to approach some more realistic scenarios of front propagation we are going to consider in this section a somewhat more generic reaction scheme in relation to front propagating in spatially modulated and noisy media [1,2].

3.1. Front propagation in spatially modulated media

In order to set the problem let us consider the evolution of a linear interface $y(x,t)$ that is moving in the y-direction and subjected to a spatial modulation in the transversal x-direction. In a broad class of systems the dynamics of an interface is given by the so-called eikonal equation, which states that the local normal velocity is equal to the planar interface velocity plus a correction coming from the curvature [27]. This result can be extended to the case in which there exists a sufficiently smooth modulation of the control parameter. Then, in terms of the local velocity $u(x)$ corresponding to the planar front solution, we have

$$v_n(x,t) = u(x) + \kappa(x,t), \tag{13}$$

where $v_n(x,t)$ is the local normal velocity and $\kappa(x,t)$ is the curvature.

In figure 11 it is shown an example of temporal evolution of the interface for a $u(x)$ with several local maxima. Starting with a planar front, a configuration with the same number of fingers is formed, which are strongly dominated by the neighborhood of the corresponding local maxima of $u(x)$. However, after this short transient a slow process of competition starts, during which some slow fingers will be eliminated and some of them will survive. The nature of this competition process is more clearly shown in figure 12, where the local velocity in the y-direction ($\partial y/\partial t$) is plotted for a particular case of a modulating function with two local maxima. Both of the fingers that appear have well defined shape and velocity. It is clearly seen how the competition between them can be described by an invasion front that advances into the slower finger, which finally disappear.

We assume that the modulation is sufficiently smooth, so we can analyze equation (13) by means of a perturbative scheme in the limit of small curvatures. This turns out to be a singular perturbation. As a result for each local maximum i of $u(x)$ there is a roughly stationary finger propagating with a velocity v^i given at the lowest order by

$$v^i = u^i_m - \sqrt{\frac{|u^{i\prime\prime}_m|}{u^i_m}} + \cdots, \tag{14}$$

where u^i_m is the maximum of $u(x)$ in the finger i, and $u^{i\prime\prime}_m$ its second derivative at the same maximum. We see that the curvature correction for the velocity of the finger is given by a length, which is nothing but the length scale of the spatial variation of the modulating function u at its local maximum.

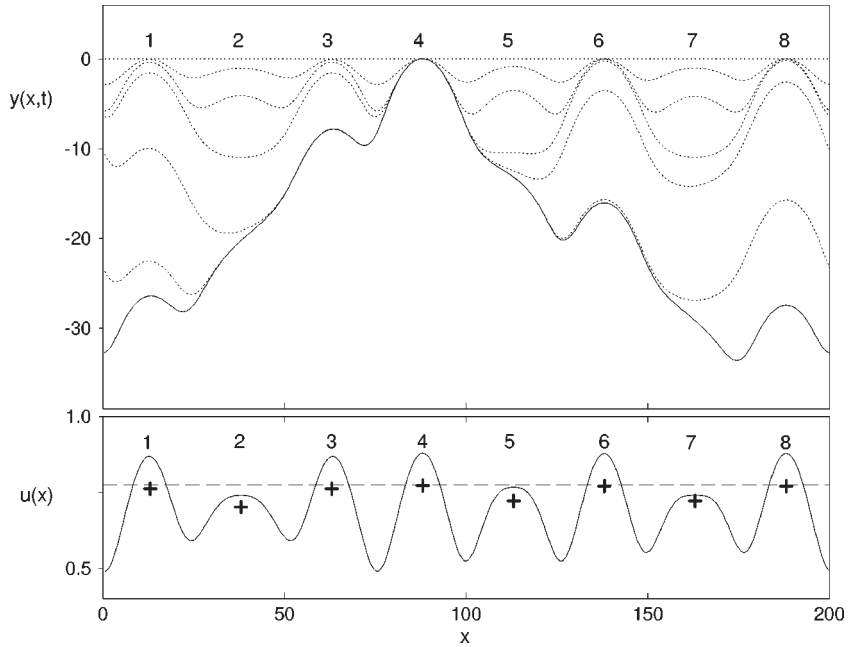

Figure 11. Temporal evolution of an initially flat front. Fronts are shown in the frame comoving with the fastest finger (4). At early times, the front $y(x,t)$ mimics the modulated local velocity $u(x)$ with 8 maxima (bottom). Three slow fingers are eliminated before the front reaches the stationary shape with only 5 fingers. The front is plotted at times: 0, 10, 20, 200, 2500, 15000 and 300000 (solid line).

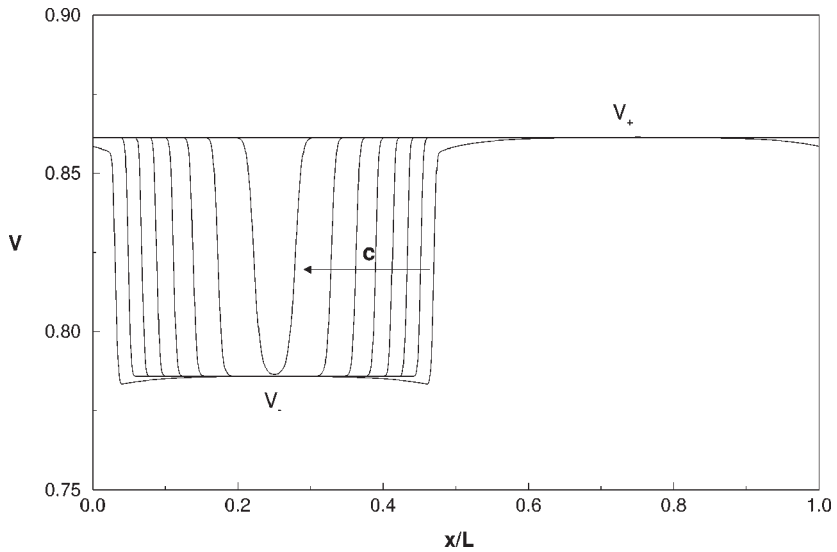

Figure 12. Competition process between two fingers. The vertical component of the local velocity of the front is plotted every $t = 50$ for the same evolution showed in figure 11. The effective transversal velocity c is also indicated.

The dynamics of finger competition can be found at the lowest order from the solution inside the boundary layers between them. We can found a stationary solution that can be seen as a one-dimensional front moving laterally at velocity c, which represents the invasion of the slower finger by the faster one. This velocity is given by their respective velocities and contact angles as

$$c = \frac{v_+ - v_-}{\tan\theta_- - \tan\theta_+}. \tag{15}$$

This represents basically a kinematic process, in which the boundary moves as dictated by the velocities of each finger.

The next point to address is the final stationary state. From the lowest order approximation, it can be shown that for smooth enough modulation, only the fastest finger given by the absolute maximum u_M of the modulating function will survive. In that case the velocity of the whole front is given by

$$v = u_M - \sqrt{\frac{|u''_M|}{u_M}} + \cdots. \tag{16}$$

The solution of the front shape for a not very smooth $u(x)$ may differ qualitatively from the lower order solution, with the existence of additional fingers. However, the number of surviving fingers (i.e., number of maxima of the stationary front shape) are given by a simple comparison between the actual selected velocity v and the local maxima of $u(x)$. The front shape will develop fingers at those maxima of $u(x)$ larger than v. A good estimate of the selected velocity v can be obtained in turn from the perturbative analysis and corresponds to the largest of the different values taken by v^i when evaluated at the different local maxima of $u(z)$.

In summary, we have seen that the steady state front velocity and the number of surviving fingers follow very simple rules found from a local analysis at the different maxima of the modulation $u(x)$.

3.2. Front propagation in noisy media

We now study the effects of external noise in a one-dimensional model of front propagation. Noise is introduced through the fluctuations of a control parameter leading to a multiplicative stochastic partial differential equation.

Our starting point is an equation of the form

$$\frac{\partial\psi}{\partial t} = \frac{\partial^2\psi}{\partial x^2} + \psi(1-\psi)(a+\psi) + \psi(1-\psi)\xi(x,t). \tag{17}$$

In this equation the coefficient of the linear term stands for an external control parameter, whose fluctuations around its mean value a are modeled by a Gaussian noise of zero mean and correlation given by

$$\big\langle \xi(x,t)\xi(x',t')\big\rangle = 2\delta(t-t')\varepsilon\left(\frac{|x-x'|}{\lambda}\right).$$

The function $\varepsilon(x)$ accounts for the spatial correlations of the external fluctuation and the parameter λ is the associated correlation length, which we take as small. The model has three homogeneous steady states $\psi = 0, 1, -a$. Their stability depends on the particular value of a, which is allowed to vary in the interval $(-1/2, 1)$ to ensure the global stability of the $\psi = 1$ state.

We are interested in the case in which a uniformly propagating front is moving to the right replacing the $\psi = 0$ state by the $\psi = 1$ state. In the absence of noise, this situation has been extensively studied in the last few years [19,20].

Analysis of simulation data reveals that the noise not only induces a shift of the ensemble averaged velocity but also a diffusive spreading of the front position. The front presents a well defined mean shape which is different from the deterministic kink solution and which is obtained when the roughness of the front is appropriately averaged out. We formally develop equation (17) in powers of the fluctuations of the front shape, and we obtain in the lower order the equation for the mean shape $p_0(x)$ of the front:

$$\frac{\partial p_0}{\partial t} = \frac{\partial^2 p_0}{\partial x^2} + p_0(1 - p_0)\big(a' + c' p_0\big), \tag{18}$$

where $a' = a + \varepsilon(0)$ and $c' = 1 - 2\varepsilon(0)$. We see in this equation that the mean front profile obeys a deterministic dynamic equation but with renormalized parameters. Therefore the selected shape and velocity of the front, within the present approximation, can be found from the known results for deterministic equations of this type.

The multiplicative noise increases the control parameter $a' > a$ and so the strength of the linear term, and it reduces the weight of the nonlinearities of the deterministic model trough the parameter $c' < 1$. Hence one could expect an increase of the propagating velocity and an increase of the domain of validity of the linear marginal-stability criterion as the intensity of the noise is increased.

As a simple linear stability analysis indicates, for $a > -\varepsilon(0)$, the $\psi = 0$ state is unstable and then a continuum of propagating velocities is possible. The minimum of them is given by the different linear and nonlinear-marginal-stability criteria. Specifically, the linear regime (L) is now delimited by the control parameter range $1/2 - 2\varepsilon(0) \leqslant a < 1$ (figure 13). In this range, any initial profile that asymptotically falls off more quickly than $\mathrm{e}^{-\kappa_{\mathrm{L}} x}$ with $\kappa_{\mathrm{L}} = \sqrt{a + \varepsilon(0)}$, propagates with the long time asymptotic velocity

$$v_{\mathrm{L}} = 2\sqrt{a + \varepsilon(0)} \tag{19}$$

and a decay κ_{L}. On the other hand, the nonlinear regime (NL) holds for $-\varepsilon(0) \leqslant a < 1/2 - 2\varepsilon(0)$ (figure 13). Here the long time asymptotic propagation velocity for initial profiles with $k \geqslant \kappa^* = (a + \varepsilon(0))/\sqrt{1/2 - \varepsilon(0)}$ is given by

$$v_{\mathrm{NL}} = \frac{2a + 1}{\sqrt{2(1 - 2\varepsilon(0))}}, \tag{20}$$

which decays with a $\kappa_{\mathrm{NL}} = \sqrt{1/2 - \varepsilon(0)}$.

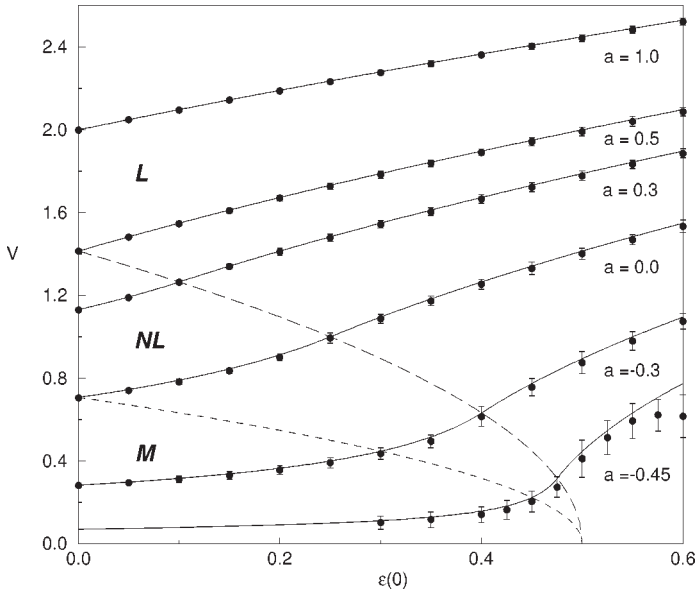

Figure 13. Front velocities versus noise intensity $\varepsilon(0)$ for several values of a. Continuous lines display analytical predictions. Dashed lines divide the different regimes. Points and their error bars correspond to numerical simulation starting from step-like profiles ($\Delta x = 0.5$ and $\Delta t = 10^{-2}$).

The multiplicative noise reduces the metastable regime (M) to the range $-(1/2) \leqslant a < -\varepsilon(0)$ (figure 13). In this case, a unique front solution is allowed with a propagating velocity given by equation (20) and κ_{NL}.

Simulation results for the front velocity are shown in figure 13 with the predictions of equations (19) and (20). The different regimes (L, NL and M) are also displayed and it is shown how the linear criterion extends its range of validity as the intensity of the noise is increased. The agreement of the theoretical prediction with the simulation results is remarkable even for large values of the intensity of the noise.

4. Front propagation in turbulent media

Let us consider a two-dimensional front propagating in a turbulent medium [12]. Here, in addition to the previously discussed length and time scales of the front propagating in a quiescent media, the spatio-temporal scales introduced by the turbulent flow will play a fundamental role. The interface, now distorted by the inhomogeneities of the media, will propagate at a different velocity v_T, which is larger than the velocity in a quiescent media v_0, to an extent that will depend singularly on the characteristics of the media.

In this way formulated, the problem is of fundamental interest when studying chemical fronts in fluid media and of special practical relevance in combustion processes [26]. However, in spite of this wide appealing, existing theoretical and experimental results are far from being totally conclusive and important discrepancies

remain in fundamental aspects such a turbulent propagation rates, velocity quenching effects, role of turbulent spectra, etc. [17].

An enlarged perspective has been gained recently when experiments on liquid phase reactions [23] have brought out a more simplified scenario as compared to that of combustion processes. In such liquid reactions the change of density and the increasing of the temperature are negligible compared with those occurring in typical combustion processes [9,18]. In this way, experimentalists are closer to reproduce the set of simplified assumptions invoked by most of the theoretical models.

In our approach we focus on front propagation under externally imposed stirring conditions. The turbulent flows are generated, independently of the front, by using a stochastic partial differential equation of Langevin type. The outline of the rest of this section is as follows. In the following section we present a brief summary of our stochastic method to generate turbulent flows. We devote section 4.2 to discuss the propagation modes observed and their proposed theoretical basis.

4.1. Turbulent media modelization

Here we summarize the basic ingredients of our scheme to generate a statistically, homogeneous, and stationary turbulent field [13]. Our starting point is a generalized Langevin equation for a stream function $\eta(\mathbf{r}, t)$,

$$\frac{\partial \eta(\mathbf{r}, t)}{\partial t} = \nu \nabla^2 \eta(\mathbf{r}, t) + Q\left[\lambda^2 \nabla^2\right] \nabla \boldsymbol{\zeta}(\mathbf{r}, t), \tag{21}$$

where ν is the kinematic viscosity and $\boldsymbol{\zeta}(\mathbf{r}, t)$ is a Gaussian white noise process of zero mean and correlation

$$\left\langle \zeta^i(\mathbf{r}_1, t_1) \zeta^j(\mathbf{r}_2, t_2) \right\rangle = 2\varepsilon_0 \nu \delta(t_1 - t_2) \delta(\mathbf{r}_1 - \mathbf{r}_2) \delta^{ij}. \tag{22}$$

In the last equations ε_0 and λ are control parameters, respectively related to the intensity and correlation length of the random flow. The differential operator $Q[\lambda^2 \nabla^2]$ is closely related with the energy spectra which can be arbitrarily chosen in our scheme. As a first example we adopt the Kraichnan's spectrum describing a distributed band of excitations around a well pronounced peak centered at a well-defined wave number k_0

$$E(k) \propto k^3 \exp\left[-k^2 \lambda^2\right]. \tag{23}$$

From the stream function the two-dimensional incompressible advecting flow with zero mean-value is obtained according to the following linear transformation:

$$\mathbf{v}(\mathbf{r}, t) = \left(-\frac{\partial \eta(\mathbf{r}, t)}{\partial y}, \frac{\partial \eta(\mathbf{r}, t)}{\partial x} \right). \tag{24}$$

The physical parameters of the flow, i.e., the stirring intensity u_0^2, the characteristic length l_0 and time t_0 scales are easily expressed in terms of the input parameters described above.

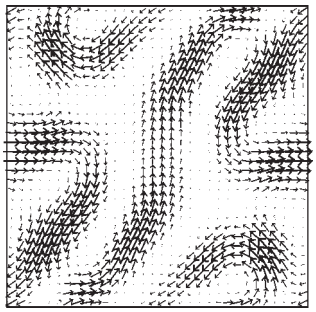

Figure 14. Pattern of a particular realization of the velocity field for the Kraichnan's spectrum. The arrows represent the velocity field painted every 4 mesh points in a normalized arbitrary scale. Parameter values: 128×128 points, lattice spacing $\Delta = 0.5$, $\varepsilon_0 = 100.0$, $\nu = 2.0$ and $\lambda = 8.0$.

The system is discretized according to standard procedures and next the temporal evolution is readily simulated in Fourier space. In figure 14 we plot a snapshot of the velocity field. The small arrows plotted every 4 mesh point indicate the local velocity field.

4.2. Turbulent front model

The next step is the formulation of the reaction–diffusion–advection scheme. We model this situation by means of a dynamical equation for a passive scalar field $\psi(\mathbf{r}, t)$ in a two-dimensional space:

$$\frac{\partial \psi}{\partial t} = D\nabla^2\psi + f(\psi) - \nabla(\mathbf{v}\psi), \tag{25}$$

where D is the molecular diffusivity, $f(\psi)$ is a nonlinear reaction term and $\mathbf{v}(\mathbf{r}, t)$ is the random flow. In our numerical simulation we have chosen $f(\psi) = \psi^2 - \psi^3$. In this case stable planar front propagates the stable state ($\psi = 1$, "products") into the invaded metastable one ($\psi = 0$, "reactants"). In the absence of stirring ($u_0^2 = 0$) two important parameters are the dimensionless propagation rate and the front thickness, which, respectively, read

$$v_0 = (D/2)^{1/2}, \qquad \delta_0 = (8D)^{1/2}. \tag{26}$$

Superposing stirring, two limiting regimes of front propagation are found in our simulations. First, when the typical length scale of the flow l_0 is larger than the intrinsic one associated to the reaction–diffusion dynamics δ_0, we observe a distorted front which propagates as a still rather sharp interface. Such a propagation mechanism is known in the combustion literature as the "thin flame," "flamelet" or "reaction sheet" regime [9,18]. Contrarily when l_0 is smaller than δ_0, we observe what is referred in the literature as a DRZ regime [9,18], i.e., a broadened front disrupted by the stirring flow. In both cases, turbulent propagation rates are larger than in quiescent media. To illustrate this phenomenology in figure 15 we display two pattern of the mentioned propagation modes.

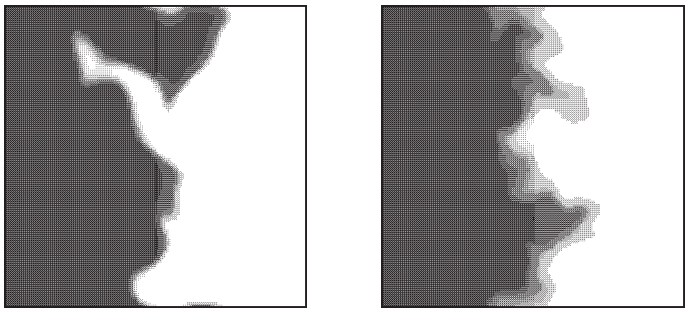

Figure 15. Density plots of the stirred reaction front propagating. Thin front mode (left, $D = 0.3$, $u_0^2 = 3.0$, $\lambda = 4.5$ and $t_0 = 1.0$), distributed reaction front regime (right, $D = 2.0$, $u_0^2 = 10.0$, $\lambda = 2.2$ and $t_0 = 1.0$).

Each one of the previously identified conditions correspond to a specific propagation mechanism. The common rationale behind the "thin flame" mode is based on a HP-like argument: the front has the same local structure as in the planar case with normal velocity given by v_0, but its length increases due to wrinkling. This results on faster propagation velocities, in such a way that the relative increment in the velocity is equal to the relative increment of increment in the velocity is equal to the relative increment of the length. This geometrical relation can be translated into quantitative arguments

$$\frac{L_T}{L_0} = \frac{v_T}{v_0}. \tag{27}$$

On the other hand, stirring is assumed to affect the velocity in the DRZ regime by solely increasing diffusive transport inside the broadened front. In this case, we simply adapt the first fundamental relation of equation (26) to obtain

$$\frac{v_T}{v_0} = \left(\frac{D_T}{D}\right)^{1/2}, \tag{28}$$

where D_T is the turbulent diffusion coefficient. These propagation modes have been observed in our numerical simulations. According to our results the arguments leading to relations (27) and (28) seem well-supported. The simplicity and versatility of the computer implementation of turbulent flows and the simple model used to describe the front propagation in these media open new perspectives in the study of more complicated situations in turbulent fluids.

Acknowledgements

The authors acknowledge discussions with J. Mai. We also thank the Centre de Supercomputació de Catalunya (CESCA) for computing support. D. Vives benefited from a FI grant from Generalitat de Catalunya. This research was jointly supported by the Dirección General de Investigación Científica y Tecnológica (DGICYT), Spain,

under Project No. PB93-0759, PB96-1001, and Comissionat per Universitats i Recerca de la Generalitat de Catalunya.

References

[1] J. Armero, A.M. Lacasta, L. Ramírez-Piscina, J. Casademunt, J.M. Sancho and F. Sagués, Europhys. Lett. 33 (1996) 429.
[2] J. Armero, A.M. Lacasta, L. Ramírez-Piscina, J. Casademunt, J.M. Sancho and F. Sagués, Phys. Rev. Lett. 76 (1996) 3045.
[3] R. Arnold, K. Showalter and J.J. Tyson, J. Chem. Educ. 64 (1987) 740.
[4] M.C. Cross and P.C. Hohenberg, Rev. Mod. Phys. 65 (1993) 851.
[5] I. Epstein and K. Showalter, J. Phys. Chem. 31 (1996) 13 132.
[6] R.J. Field and M. Burger, eds., *Oscillations and Traveling Waves in Chemical Systems* (Wiley, New York, 1985).
[7] P. Fife, J. Chem. Phys. 64 (1976) 554.
[8] R.A. Fisher, Ann. Eugenics 7 (1937) 355.
[9] B.D. Haslam and P.D. Ronney, Phys. Fluids 7 (1995) 1931.
[10] A. Kolmogorov, I. Petrovsky and N. Piskunov, Bull. Univ. Moscow, Int. Ser. Sec. A 1 (1937) 1; translated in P. Pelc, *Dynamics of Curved Fronts* (Academic Press, San Diego, 1988).
[11] R. Luther, Elektrochem. 12 (1906) 596; translated and discussed in [3].
[12] A. Martí, F. Sagués and J.M. Sancho, Phys. Rev. E (accepted).
[13] A.C. Martí, J.M. Sancho, F. Sagués and A. Careta, Phys. Fluids 9 (1997) 1078.
[14] J.D. Murray, *Mathematical Biology* (Springer, Berlin, 1989).
[15] P. Ortoleva and J. Ross, J. Chem. Phys. 63 (1975) 3398.
[16] M. Otwinowski, P. Paul and W.G. Laidlaw, Phys. Lett. A 128 (1988) 483.
[17] P.D. Ronney, in: *Modeling in Combustion Science*, J. Buckmaster and T. Takeno, eds., Lectures Notes in Physics, Vol. 449 (Springer, Berlin, 1995).
[18] P.D. Ronney, B.D. Haslam and N.O. Rhys, Phys. Rev. Lett. 74 (1995) 3804.
[19] W. van Saarloos, Phys. Rev. Lett. 58 (1987) 271; Phys. Rev. A 37 (1988) 211.
[20] W. van Saarloos, Phys. Rev. A 39 (1989) 6367.
[21] E.E. Sel'kov, Eur. J. Biochem. 4 (1968) 79.
[22] K. Showalter and J.J. Tyson, J. Chem. Educ. 64 (1987) 742.
[23] S.S. Shy, P.D. Ronney, S.G. Buckley and V. Yakhot, in: *Proceedings of the 24th Symposium (International) on Combustion* (Combustion Institute, Pittsburgh, 1992).
[24] D. Vives, A. Careta and F. Sagués, J. Chem. Phys. 107 (1997) 7894.
[25] X.Y. Wang, Phys. Lett. A 131 (1988) 277.
[26] F.A. Williams, *Combustion Theory*, 2nd edn. (Benjamin-Cummins, Menlo Park, CA, 1985).
[27] V.S. Zykov, Biophysics 25 (1980) 906.